End-to-End Distance Distributions of Flexible Molecules: Frequency-Domain Fluorescence Energy Transfer Measurements and Rotational Isomeric State Model Calculations

Joseph R. Lakowicz,[*,†] **Wieslaw Wiczk,**[†] **Ignacy Gryczynski,**[†] **Mayer Fishman,**[†] **and Michael L. Johnson**[‡]

Department of Biological Chemistry, School of Medicine, University of Maryland at Baltimore, 108 North Greene Street, Baltimore, Maryland 21201, and the Department of Pharmacology, University of Virginia, Charlottesville, Virginia 22908

ABSTRACT: We used frequency-domain measurements of fluorescence energy transfer to determine the end-to-end distance distribution of donor–acceptor (D–A) pairs linked by flexible alkyl chains. The length of the linker was varied from 11 to 28 atoms, and two different D–A pairs were used. In each case the D–A distributions were recovered from global analysis of measurements with different values for the Förster distance, which were obtained by collisional quenching of the donors. In all cases essentially the same distance distribution was recovered from the frequency-domain data for each value of the Förster distance. Additionally, these recovered distributions were also in agreement with those recovered from steady-state measurements of the energy-transfer efficiency for various Förster distances. We compared the experimentally recovered distance distributions with those calculated from the rotational isomeric state (RIS) model of Flory. The experimentally recovered distance distributions for the largest chain molecules were in agreement with the predictions of the RIS model. However, the experimental and RIS distributions were distinct for the shorter D–A pairs. The experimental distance distributions were not in agreement with the predictions of two simpler models, the freely jointed and the freely rotating chain models. Overall, these results demonstrate that the current resolution of distance distributions is adequate for comparison with the results of conformational modeling, which in turn should allow refinement of these models.

Introduction

Nonradiative or fluorescence resonance energy transfer has been widely used to measure the distances between sites on biological macromolecules.[1-3] These measurements are possible because the high sensitivity of fluorescence methods allows measurements on dilute solutions and because the characteristic distance for energy transfer (the Förster distance, R_0) is typically near 30 Å,[4] which is comparable to the dimension of proteins and membranes. The most common application of fluorescence resonance energy transfer (FRET) has been to systems such as native proteins, for which one expects a single conformational state and a single donor (D) to acceptor (A) distance.

In the present report we describe a generalization of the FRET measurements to allow resolution of a distribution of D–A distances. Briefly, the rate of D-to-A transfer depends upon the D-to-A distance. A range of D–A distances results in a range of transfer rates, which in turn results in a range of decay times for the excited-state donor population. We recovered the intensity decays of the donor using the frequency-domain (FD) method.[5-7] The frequency response of the donor emission was used to recover the distribution of D–A distances. To improve the resolution, we performed a global analysis of data obtained at various R_0 values, which were obtained by using collisional quenching of the donors.[8,9] By varying R_0 the FD measurements become sensitive to different parts of the D-to-A distribution, and the global analysis fits all these data to a single distance distribution. Additionally, the dependence of the steady-state energy transfer on R_0 was used as an independent measure of the distance distributions.

We examined two series of D–A pairs, each with nearly identical flexible spacers of varying lengths. The first series used an indole residue as the donor (Chart I, top), which was provided by condensation of tryptamine (TA) with various acceptors. The second series used a naphthalene residue as the donor (Chart I, bottom), which was synthesized from 1-naphthalenemethylamine (NMA). The flexible spacers varied in length from 11 atoms (C, N, or S) to 28 atoms. For both series of D–A pairs the acceptor was a dansyl residue linked via a sulfonamide bond. The flexible spacers of both series of D–A pairs are similar in length and structure; the use of two donors provides the opportunity to recover the end-to-end distribution from separate experiments and thereby check for consistency. Additionally, the decay times of the TA and NMA residues differ 10-fold, 6.5 and 65.7 ns, respectively. This difference will be useful in future and ongoing studies of end-to-end diffusion in solvents of varying viscosity.[11,12] It should be noted that this work is an extension of the pioneering work of Haas, Steinberg, and co-workers. These researchers used time-domain fluorescence methods to examine end-to-end distribution of peptides,[13,14] including the estimation of end-to-end diffusion coefficients.[15,16]

We compared these experimentally recovered distance distributions with those calculated from the statistics of flexible chain molecules.[10] In particular, the rotational isomeric state (RIS) model of Flory[10] was used to calculate the D-to-A distributions. This model describes each bond as having a particular angular geometry and for simplicity allows only a limited number of rotational isomers about the single bonds. The relative proportion of the rotational isomers is given by Boltzmann factors. These calculated distributions were compared with those obtained from the FD data. We also compared our data to the distributions predicted for freely jointed and freely rotating chains.[10] In general we found that the freely jointed and rotating models did not predict distributions which were consistent with the experimental data. The RIS model yielded distinctly superior predictions. However, the predictions of the RIS model were found to agree with the

* Corresponding author.
‡ University of Virginia.
† University of Maryland at Baltimore.

**Chart I
Donor–Acceptor Pairs[a]**
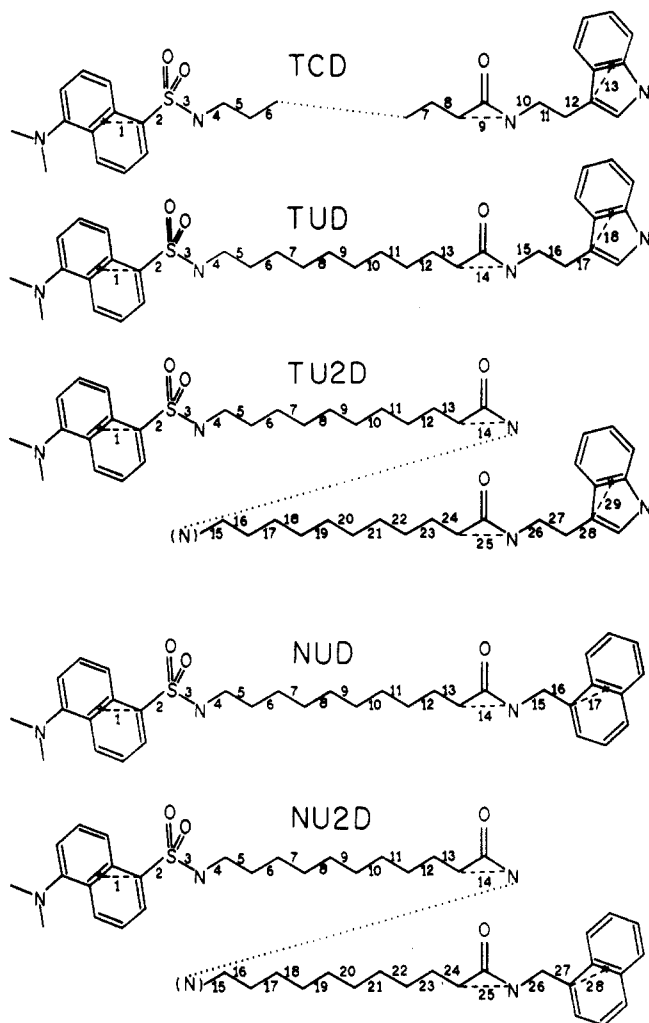
[a] The bond numbers refer to the RIS calculations (Table III).

experimental distributions only for the chains longer than ~20 carbons.

Theory

Single-Exponential Donor Decays. The theory of energy transfer in the presence of a distance distribution is moderately complex. We first describe the simpler case where the donor decay, in the absence of acceptor, is a single exponential. This is the case for both donors (TA and NMA residues) used in the present report. However, the donor decays in the absence of acceptor become multi- or nonexponential in the presence of collisional quenching because of the transient effects in diffusive quenching. Hence, we also describe the theory for a multiexponential donor (below).

Assume the decay of the donor ($I_D(t)$), in the absence of energy transfer or quenching, is a single exponential

$$I_D(t) = I_D^\circ \exp[-t/\tau_D^\circ] \qquad (1)$$

where τ_D° is the decay time of the donor. The superscript $^\circ$ indicates the absence of collisional quenching. Consider a single D–A pair in which the acceptor is present at a unique distance r. The donor decay of this molecule with a unique D–A distance is given by

$$I_{DA}(r,t) = I_D^\circ \exp[-t/\tau_D^\circ - k_{DA}t] = I_D^\circ \exp[t/\tau_{DA}] \qquad (2)$$

The rate of energy transfer is dependent on the D–A

distance and given by

$$k_{DA} = 1/\tau_D^\circ (R_o/r)^6 \qquad (3)$$

where R_o is the Förster distance. When an acceptor is present at a single distance, the donor decay remains a single exponential, and the intensity decay rate is given by

$$1/\tau_{DA} = 1/\tau_D^\circ + k_{DA} \qquad (4)$$

The Förster distance R_o can be calculated from the spectral properties of the chromophores[17]

$$R_o^6 = \frac{9000(\ln 10)\kappa^2 \phi_D^\circ}{128\pi^5 N n^4} \int_0^\infty F_D(\lambda)\, \epsilon_A(\lambda)\, \lambda^4\, d\lambda \qquad (5)$$

where κ^2 is the orientation factor, ϕ_D° the quantum yield of the donor in the absence of acceptor and quencher, n the refractive index of the intervening solvent, N Avogadro's number, $F_D(\lambda)$ the emission spectrum of the donor with the area normalized to unity, $\epsilon_A(\lambda)$ the absorption spectrm of the acceptor (in units of M^{-1} cm^{-1}), and λ the wavelength (in nm). The distances recovered from energy-transfer measurements may be uncertain due to the unknown orientation of the D–A pairs[18] or to any end-to-end diffusion during the lifetime of the excited state. To minimize these effects we used solvents of modest viscosity which minimize the extent of D–A diffusion during the excited-state lifetime (see below). However, the solvents were sufficiently fluid to allow angular displacements of the donors and acceptors, resulting in averaging of the orientation effects and less uncertainty in the distance distribution. Hence, the value of κ^2 was assumed to be equal to $^2/_3$ due to the range of conformations, the occurrence of significant rotational diffusion during the donor lifetime, and the mixed polarization of the chromophores.[19]

The intensity decay of the donor becomes more complex if the acceptor is located over a range of D–A distances, as is expected for our flexible D–A pairs. Since each individual D–A pair is characterized by a specific distance r, the intensity decay of each donor is still a single exponential, given by

$$I_{DA}(r,t) = I_D^\circ \exp\left[-\frac{t}{\tau_D^\circ} - \frac{t}{\tau_D^\circ}\left(\frac{R_o}{r}\right)^6\right] \qquad (6)$$

However, the observed decay contains contributions from D–A pairs at all accessible distances and is thus more complex than a single exponential. The intensity decay of the ensemble of D–A pairs is given by the average of the individual decays weighted by the distance probability distribution ($P(r)$) of the D–A pairs.[15,16,20,21]

$$I_{DA}(t) = I_D^\circ \int_0^\infty P(r) \exp\left[\frac{t}{\tau_D^\circ} - \frac{t}{\tau_D^\circ}\left(\frac{R_o}{r}\right)^6\right] dr \qquad (7)$$

This expression is appropriate for a distribution in which the D–A distances are static during the donor decay. To maintain this condition the tryptamine series was examined in propylene glycol at 20 °C and the naphthalene series at -5 °C.

The extent of end-to-end diffusion can be estimated from the donor decay times and the solvent viscosity. In the presence of acceptor, the mean decay times ($\bar{\tau}$) of the tryptamine and naphthalene series are near 2 and 18 ns, respectively (see Tables V and VI). The mean distance

for diffusion (Δx^2) can be estimated from

$$\Delta x^2 = 2D\bar{\tau} \tag{8a}$$

where the diffusion coefficient (D) is estimated by the Stokes–Einstein relationship

$$D = kT/6\pi\eta R \tag{8b}$$

and k is the Boltzmann constant, η the viscosity, and R the radius of the diffusing moiety. The viscosities of propylene glycol are near 48 and 294 cP at 20 and –5 °C, respectively. Hence, based on $R = 5$ Å, the mean displacements are expected to be near 2.7 and 3.1 Å for indole and naphthalene, respectively. In this calculation we used the sum of the donor and acceptor diffusion coefficients, that is, $D = D_D + D_A$. Furthermore, we subsequently developed programs which allow the distance distributions to be recovered in the presence of D-to-A diffusion.[11,12] We found that diffusion had a negligible effect on the recovered distributions for the D–A pairs under the stated experimental condition (unpublished observation).

Distance Distributions. In this report we assume that the probability distribution is a truncated Gaussian

$$\begin{cases} P(r) = \dfrac{1}{Z} \exp\left[-\dfrac{1}{2}\left(\dfrac{r-\bar{r}}{\sigma}\right)^2\right] & \text{for } r_{\min} \le r \le r_{\max} \\ P(r) = 0 & \text{for } r < r_{\min} \text{ and for } r > r_{\max} \end{cases} \tag{9a}$$

in which the normalization factor, Z, is given by

$$Z = \int_{r_{\min}}^{r_{\max}} \exp\left[-\dfrac{1}{2}\left(\dfrac{r-\bar{r}}{\sigma}\right)^2\right] dr \tag{9b}$$

where $\bar{r}$ is the average and σ the standard deviation of the untruncated Gaussian distribution. The meaning of $P(r)$ is taken to be the probability that an acceptor is present in the interval r to $r + dr$, so that the distance-dependent volume element is contained in $P(r)$ and is analogous to the end-to-end radial distribution function described by Zimmt et al.[39] We report the widths of the distributions in terms of the half-widths (hw, full width at half-maximum), which is related to σ by hw $= 2.354\sigma$.[22] We note that the Gaussian may not be the theoretically correct form for the distance distribution. However, we found that this model was adequate to account for the data. Additionally, with few exceptions,[23] we were not able to recover more complex distance distributions from these experimental data. Our rationale for selecting this form for $P(r)$, and its relationship to Flory's $W(\bar{r})$, is given in the Appendix. We note that theoretical calculations of an end-to-end radial distribution function for short-chain molecules result in nearly Gaussian shapes.[39]

Frequency-Domain Expressions. The intensity decays of the donor emission were measured using the frequency-domain method. The experimental values are the phase (ϕ_ω) and modulation (m_ω) of the emission over a range of modulation frequencies (ω), where $\omega = 2\pi \times$ frequency in cycles per second (Hz). Irrespective of the form of the intensity decay $I(t)$ the frequency response can be predicted using

$$N_\omega = \dfrac{\int_0^\infty I(t) \sin \omega t \, dt}{\int_0^\infty I(t) \, dt} \tag{10}$$

$$D_\omega = \dfrac{\int_0^\infty I(t) \cos \omega t \, dt}{\int_0^\infty I(t) \, dt} \tag{11}$$

The calculated (c) phase and modulation values for the assumed decay law are given by

$$\phi_{c\omega} = \arctan\, [N_\omega/D_\omega] \tag{12}$$

$$m_{c\omega} = [N_\omega^2 + D_\omega^2]^{1/2} \tag{13}$$

It is informative to analyze the frequency responses of the donor controls and the D–A pairs using the multiexponential model

$$I(t) = \sum_i \alpha_i \exp[-t/\tau_i] \tag{14}$$

where α_i are the preexponential factors and τ_i the associated decay times. The multiexponential analysis of the D–A pair donor decays reveals the extent of heterogeneity due to the D–A distance distribution. Additionally, the parameterized form of the donor-alone decay time is also needed for calculation of the distance distributions (eqs) 17, 18, 25, and 26), particularly where the donor-alone decay becomes nonexponential due to collisional quenching. For the multiexponential model the transforms (eqs 10 and 11) can be represented analytically[24,25]

$$N_\omega = \dfrac{1}{J}\sum_i \dfrac{\alpha_i \omega \tau_i^2}{1 + \omega^2 \tau_i^2} \tag{15}$$

$$D_\omega = \dfrac{1}{J}\sum_i \dfrac{\alpha_i \tau_i}{1 + \omega^2 \tau_i^2} \tag{16}$$

where the normalization factor is given by $J = \sum_i \alpha_i \tau_i$. For a distribution of D–A distances, the transforms are calculated numerically, using

$$N_\omega = \dfrac{1}{J}\int_{r=r_{\min}}^{r_{\max}} \dfrac{P(r)\tau_{DA}^2}{1 + \omega^2 \tau_{DA}^2} \, dr \tag{17}$$

$$D_\omega = \dfrac{1}{J}\int_{r=r_{\min}}^{r_{\max}} \dfrac{P(r)\tau_{DA}}{1 + \omega^2 \tau_{DA}^2} \, dr \tag{18}$$

where the normalization factor J is given by

$$J = \left(\int_{t=0}^\infty I_{DA}(t) \, dt\right) \tag{19}$$

It should be remembered that eqs 17 and 18 contain τ_{DA}, which is itself dependent upon the D–A distance (eqs 3 and 4). We also note that the integrals over distance (eqs 17–19) are typically calculated from some minimum distance ($r_{\min}$) near 2 Å to a maximum ($r_{\max}$) of ~50 Å. This range is adequate to account for the range of accessible distances, and in general, the results of the analyses did not depend upon the precise values of the minimal and maximal distances.

The parameters describing the intensity decay (α_i and τ_i or $\bar{r}$ and σ) are found using nonlinear least-squares

fitting.[22,26,27] The parameter values are estimated by minimizing $\chi_R{}^2$

$$\chi_R{}^2 = \frac{1}{\nu}\sum_{\omega,Q}\left[\frac{\phi_\omega - \omega_{c\omega}}{\delta\phi}\right]^2 + \frac{1}{\nu}\sum_{\omega,Q}\left[\frac{m_\omega - m_{c\omega}}{\delta m}\right]^2 \quad (20)$$

where ν is the number of degrees of freedom (number of data minus the number of free parameters). Where needed, the sum extends over the data sets for all quencher (Q) concentrations to provide a global analysis with multiple values of R_0 (see below). The weighing factors $\delta\phi = 0.2°$ and $\delta m = 0.005$ are the experimental uncertainties in the measured phase and modulation values. These values are estimated from our experience with the FD measurements and instrumentation over a period of several years, and these values give approximate equal weight to the phase and modulation data. The minimum value of $\chi_R{}^2$ may not be precisely unity for a given data set because of variations in $\delta\phi$ and δm between individual measurements. However, the relative values of minimized $\chi_R{}^2$ obtained for a given set of data and different models can be compared without ambiguity.

Estimation of the uncertainties in the recovered parameters is a difficult problem. Correlation allows the parameter values to vary in a concerted manner without significantly affecting the value of $\chi_R{}^2$. We used two different methods, each of which resulted in similar estimated uncertainties. Our analysis programs calculate the uncertainties by examination of the range of parameter values which are consistent with the data, using a method which partially accounts for correlation between the parameters.[26,27] We also examined the dependence of $\chi_R{}^2$ surfaces for fixed values of the parameters followed by adjustment of the other values to minimize $\chi_R{}^2$. The latter method should completely account for correlation between the parameters because these values are allowed to vary as needed to minimize $\chi_R{}^2$.

Multiexponential Donor Decays. We used collisional quenching to decrease the quantum yield of the donor and thereby vary R_0 (eq 5). The multiexponential model was used to describe the donor decays in the absence of acceptor but in the presence of quencher. In the presence of collisional quenching the intensity decays of the donors become nonexponential due to transient effects in quenching,[28-31] and this effect is adequately accounted for by the multiexponential model. The decays of the donor-alone controls (TMA and NOA; Figure 1) were fit using a sum of exponentials

$$I_D{}^Q(t) = \sum_i \alpha_{Di}{}^Q \exp[-t/\tau_{Di}{}^Q] \quad (21)$$

where $\alpha_{Di}{}^Q$ are the preexponential factors and $\tau_{Di}{}^Q$ the associated decay times. The superscript Q indicates the collisional quencher. We assumed that the Förster distance for transfer from each component in the donor decay is the same and the transfer rates are proportional to the decay rates of each component. Hence, the transfer rates are given by

$$k_{DAi}{}^Q = \frac{1}{\tau_{Di}{}^Q}\left(\frac{R_0{}^Q}{r}\right)^6 \quad (22)$$

and the distance-dependent donor decay times are given by

$$\frac{1}{\tau_{DAi}{}^Q} = \frac{1}{\tau_{Di}{}^Q} + \frac{1}{\tau_{Di}{}^Q}\left(\frac{R_0{}^Q}{r}\right)^6 \quad (23)$$

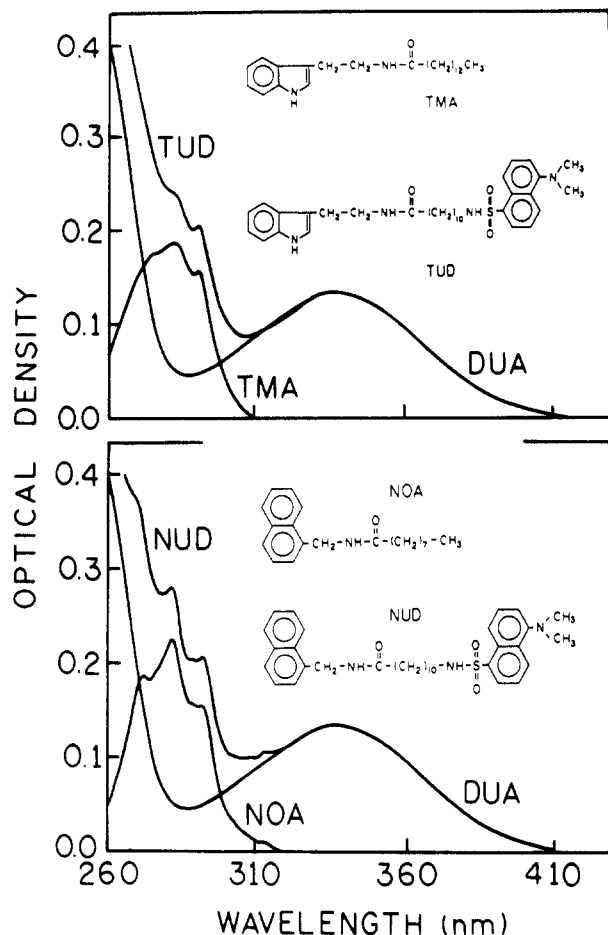where $R_0{}^Q$ is the Förster distance appropriate for a given

Figure 1. Absorption spectra of representative donors, acceptors, or D–A pairs. Top: Absorption spectra of the donor (TMA), acceptor (DUA), and a D–A pair (TUD). Bottom: Absorption spectra of the donor (NOA), acceptor (DUA), and a D–A pair (NUD).

concentration of quencher (below). We recognize that eq 22 may not be strictly correct and that one could alternatively assume that quenching does not affect the rate of energy transfer. However, our experiments do not distinguish between these alternatives. Additionally, the same distance distributions were recovered without and with the external quencher, where the intensity decays are single and multiexponentials, respectively. Hence, it appears that this assumption (eq 22) does not significantly affect the recovered distance distributions.

The intensity decay for an ensemble of D–A pairs in the presence of collisional quenching is given by

$$I_{DA}{}^Q(t) = \int_0^\infty P(r)\sum_i \alpha_{Di}{}^Q \exp\left[-t/\tau_{Di}{}^Q - \frac{t}{\tau_{Di}{}^Q}\left(\frac{R_0{}^Q}{r}\right)^6\right] dr \quad (24)$$

The sine and cosine transforms are

$$N_\omega{}^Q = \int_0^\infty \sum_i \frac{P(r)\alpha_{Di}\omega(\tau_{DAi}{}^Q)^2}{1 + \omega^2(\tau_{DAi}{}^Q)^2} dr \quad (25)$$

$$D_\omega{}^Q = \int_0^\infty \sum_i \frac{P(r)\alpha_{Di}\tau_{DAi}{}^Q}{1 + \omega^2(\tau_{DAi}{}^Q)^2} dr \quad (26)$$

We note that a multiexponential decay for the donor does not introduce additional parameters into the analysis. This is because the intrinsic decays of the donor are measured

in a separate experiment, using donors without an acceptor in the presence of the collisional quencher. The data from the donor are fit using the multiexponential model (eq 21), and the parameters ($\alpha_{Di}{}^Q$ and $\tau_{Di}{}^Q$) are held constant in eqs 25 and 26 during least-squares analysis. Once again, notice that $\tau_{DAi}{}^Q$ depends on distance (eq 23).

Dependence of the Förster Distance on Collisional Quenching. The ability to recover a distance distribution depends upon the value of R_o, which defines the range of distances over which the transfer is significantly dependent upon distance. We expanded the detectable range of distances using collisional quenching of the donor, which decreases the quantum yield and thereby decreases R_o (eq 5). We previously demonstrated that the appropriate quantum yields are given by the dynamic or collisional component in the quenching.[8,9] Hence, the appropriate quantum yields are given by

$$\phi_D{}^Q = \phi_D{}^\circ/(1 + K_D[Q]) \tag{27}$$

where $\phi_D{}^\circ$ is the quantum yield in the absence of quenching, K_D the dynamic quenching constant, and [Q] the concentration of quencher. This component was found from plots of

$$K_{app} = \frac{I_D{}^\circ/I_D - 1}{[Q]} = (K_S + K_D)[Q] + K_S K_D[Q]^2 \tag{28}$$

where $I_D{}^\circ$ and I_D are the steady-state donor intensities in the absence and presence of quenching, respectively, [Q] is the quencher concentration, and K_S is the static component of the quenching. K_S and K_D are calculated from the quadratic equation and the slope and intercept of the plot. The quenching-dependent Förster distances are then given by

$$R_o{}^Q = R_o(\phi_D{}^Q/\phi_D{}^\circ)^{1/6} \tag{29}$$

Frequency-domain data measured at a single value of $R_o{}^Q$ can be analyzed using eqs 25 and 26 with the appropriate value of $R_o{}^Q$. In general, the frequency-domain data for a single value of $R_o{}^Q$ are adequate to determine the D–A distance distributions. Nonetheless, to improve the reliability of these distributions we performed global analysis of the FD data recovered for a range of quencher (and $R_o{}^Q$) values. In this case the sum in eq 20 extends over both the measured frequencies (ω) and the quencher (Q) concentrations.

Distance Distributions from Steady-State Energy Transfer. An independent estimate of the distance distribution was obtained from steady-state measurements of the transfer efficiency (E^Q) as the Förster distance is varied by quenching.[8,9] For an assumed distance distribution, the efficiency of transfer can be calculated using

$$E_c{}^Q = \int_{r=r_{min}}^{r_{max}} \frac{P(r)(R_o{}^Q)^6}{(R_o{}^Q)^6 + r^6} \, dr \tag{30}$$

The parameters describing the assumed distance distribution are varied to yield the minimum value of $\chi_R{}^2$

$$\chi_R{}^2 = \frac{1}{\nu}\sum_Q \left(\frac{E^Q - E_c{}^Q}{\Delta E}\right)^2 \tag{31}$$

where E^Q are the measured transfer efficiencies at each $R_o{}^Q$ value, $\Delta E = 0.01$ is the estimated error in the measured efficiencies (E^Q), and ν is the number of degrees of freedom.

The transfer efficiency is given by

$$E^Q = 1 - \frac{I_{DA}{}^Q}{I_D{}^Q} \tag{32}$$

where I_{DA} and I_D are the donor fluorescence intensities for the donor–acceptor pair and the donor alone, respectively, each measured at the same quencher concentration.

Materials and Methods

Instrumentation and Measurements. Frequency-domain measurements were performed on the instrument previously described in detail.[6,7] The excitation source was a 3.79-MHz train of pulses, ~7 ps wide, obtained from the cavity-dumped output of a rhodamine 6G dye laser, which was synchronously pumped with a mode-locked argon ion laser. The dye laser output was frequency-doubled to 293 nm for excitation of the naphthalene donor and to 295 nm for excitation of the indole donor. This source is intrinsically modulated to many gigahertz and is used directly to excite the sample. The modulated emission was detected using a microchannel plate photomultiplier tube, R1564U (Hamamatsu Corp.), which was externally cross-correlated.[7] All intensity decays were measured using rotation-free polarization conditions. The donor emission was selected using an interference filter with a 10-nm band pass, centered at 340 nm for naphthalene at 360 nm for indole.

All compounds were purified by HPLC just prior to preparation of the samples for measurement. All solutions were in propylene glycol, with optical densities near 0.3 or lower at the excitation wavelength. For the naphthalene-containing samples the solutions were purged with nitrogen to remove dissolved oxygen. Emission spectra were recorded on all samples and blanks, and these spectra indicated the absence of signals due to impurities in the solvent. The measurements were performed at –5 °C for the naphthalene series and 20 °C for the indole series. These temperatures were chosen to allow for significant collisional quenching by triethylamine or acrylamide but to provide viscosities sufficient to prevent significant end-to-end diffusion during the excited-state lifetimes.

Quantum yields of the donors were measured relative to a value of 0.13 for tryptophan in water at 20 °C,[32] using a refractive index of $n = 1.4324$ for propylene glycol. The quantum yield of NOA was found to be 0.21 at –5 °C and 0.18 at 20 °C in propylene glycol. The quantum yield of TMA was found to be 0.445 at 20 °C and 0.483 and –5 °C.

Synthesis of Dansyl Amino Acids. *N*-Dansyl-6-amino-caproic acid (DCA) or *N*-dansyl-11-aminoundecanoic acid (DUA) was synthesized as follows. The amino acid (6-aminocaproic acid, CA; or 11-aminoundecanoic acid, UA; 1.6 mmol) was dissolved in 5 mL of 1 M NaHCO₃, to which was added 100 mg (0.37 mmol) of dansyl chloride (DNS-Cl) in 4 mL of acetone and 0.2 mL of triethylamine (Et₃N). The solution was stirred for 15 min, acidified to pH 3 with 2 N HCl, and extracted 3× with ethyl acetate. The ethyl acetate was pooled, washed with water, dried over MgSO₄, and evaporated in a vacuum. The crude product was purified by thin-layer chromatography on preparative silica gel plates using ethyl acetate–hexane as the developer.

N-**(Dansyl-6-aminocaproyl)tryptamine (TCD).** DCA (1 mmol), tryptamine (TA; 1 mmol), and Et₃N (2.4 mmol) were dissolved in 3 mL of dimethylformamide (DMF) in an ice bath. Bis(2-oxo-3-oxalidinyl)phosphinic chloride (BOP-Cl; 1.2 mmol) was added with stirring, which was continued overnight at room temperature. The reaction mixture was diluted with ethyl acetate, washed with 1 N HCl (3×), saturated KHCO₃ (3×), and saturated NaCl (3×), dried with Na₂SO₄, and evaporated under vacuum. The crude product was purified on a preparative silica gel plate, followed by reverse-phase HPLC on a C₁₈ column using methanol–water mixtures.

(*tert*-**Butoxycarbonyl)undecanoic Acid (t-Boc-UA).** 11-Aminoundecanoic acid (2 mmol) was dissolved and stirred in a mixture of *tert*-butanol (3 mL) and 2 N NaOH (3 mL) in an ice bath. Di-*tert*-butyl dicarbonate (BDC; 2.2 mmol) was added and stirred, and stirring continued overnight at room temperature. Excess BDC was extracted with hexane. The solution was then cooled in an ice bath, covered with a layer of ethyl acetate, and

acidified to pH 2-3 with 1 N HCl. The aqueous phase was extracted 2× with ethyl acetate, pooled, dried over anhydrous Na₂SO₄, and evaporated under vacuum.

N-(*tert*-Butoxycarbonyl)undecanoyltryptamine (t-Boc-TUA). t-Boc-UA (1 mmol) was dissolved in 4 mL of dimethylformamide, in an ice bath, to which were added 1.2 mmol of 1-hydrobenzotriazole (HOBT), 1.2 mmol of dicyclohexylcarbodiimide (DCC), and 1.1 mmol of tryptamine. The reaction was continued overnight at room temperature with stirring. The solution was diluted with ethyl acetate and the urea removed by filtration. The filtrate was washed with 1 N HCl, with 5% NaHCO₃, and with saturated NaCl, followed by drying with Na₂SO₄. The solvent was removed under vacuum, and the crude product was purified on a silica gel preparative thin-layer plate using ethyl acetate-hexane.

(11-Aminoundecanoyl)tryptamine (TUA). The t-Boc protecting group was removed using 4 N HCl in dioxane for 1 h. The solvent was evaporated under vacuum.

Synthesis of TUD and TU2D (Chart I). TUD was synthesized by coupling DUA with TA, using BOP-Cl, as described for TCD. TU2D was synthesized in the same way, using DUA and TUA as the starting compounds. The products were purified by thin-layer chromatography followed by C₁₈ reverse-phase HPLC.

Myristoyltryptamine (TMA). The donor was N-myristoyltryptamine (TMA). This compound was synthesized by coupling tryptamine to myristic anhydride in tetrahydrofuran. Myristic anhydride was formed by refluxing with acetic anhydride, followed by removal of the excess anhydride under vacuum. The TMA product was purified by HPLC.

Naphthalene-Containing D-A Pairs. Synthesis of NOA or (11-aminoundecanoyl)-1-naphthylenemethylamine (NUA) was accomplished by condensation of 1-naphthylenemethylamine (NMA) with the octanoic acid as t-BocUA using DCC as the condensing agent. NOA was synthesized by dissolving 1 mmol of octanoic acid in DMF with 2 mmol of HOBT, 1 mmol of Et₃N and 1 mmol of DCC. The solution was stirred for 30 min at 0 °C, followed by addition of 1 mmol of NMA and overnight stirring at room temperature. The product was extracted into ethyl acetate, which was washed with 1 N HCl (3×), 1 M KHCO₃ (3×), and saturated NaCl (3×), followed by drying with anhydrous MgSO₄. The product was isolated using preparative silica gel plates using ethyl acetate-hexane (1:1), followed by reverse-phase HPLC on a C₁₈ column using methanol-water.

NUA was synthesized by reacting t-Boc-UA with NMA, as described above for NOA. The t-Boc protecting group was removed in HCl-dioxane, followed by removal of the solvent under vacuum.

NUD and NU2D (Chart I). NUD was synthesized by reacting of 1.6 mmol of NUA (in 2 mL of 1 M NaHCO₃) with 2.0 mmol of DNS-Cl (in 8 mL of acetone). The mixture was stirred overnight and acidified with 1 N HCl and the product extracted into ethyl acetate. The product (NUD) was purified by silica gel thin-layer chromatography (ethyl acetate-hexane, 1.5:1) and C₁₈ reverse-phase HPLC (methanol-water).

NU2D was synthesized by the condensation of NUA (1 mmol) with DUA (1 mmol) in 4 mL of DMF, which contained 1.2 mmol of BOP-Cl and 2 mmol of Et₃N, followed by extraction, washing, and HPLC purification.

Results

Absorption and Emission Spectra. Absorption spectra of the donors, acceptors, and representative D-A pairs are shown in Figure 1. In each case the absorption spectrum of the D-A pair is the sum of that found for the donor (TMA or NOA) and the acceptor (DUA). The donors are easily excited at 295 nm, which is a region of high donor absorption and minimal acceptor absorption. Direct excitation of some acceptor fluorescence does not cause any difficulty because we isolate the donor emission using interference filters.

Emission spectra of the tryptamine and naphthalene series are shown in Figure 2. The donor emission maxima are near 360 nm for the indole residue (A) and 340 nm for
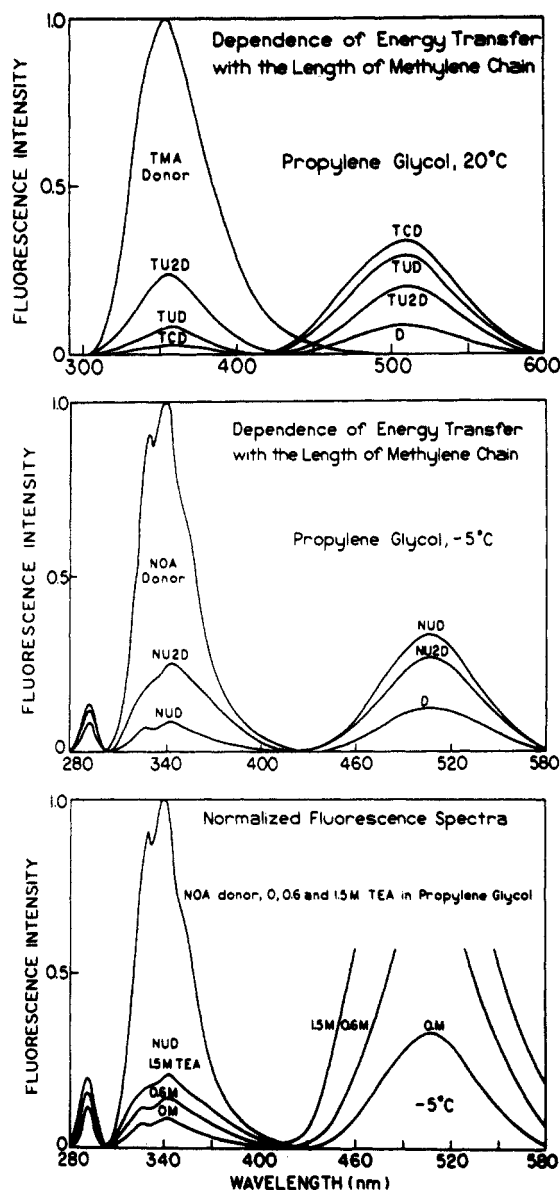

Figure 2. Emission spectra of the tryptamine (A, top) and naphthalene (B, middle) series of D-A pairs. (C, bottom) Emission spectra of NOA and NUD in the absence and presence of TEA. D is dansylamide.

the naphthalene residue (B). These maxima are well-separated from the emission due to the acceptor, which is centered near 510 nm. The absence of overlap of the emission from the donor and acceptor allows the donor emission to be isolated using interference filters centered at 360 and 340 nm, for indole and naphthalene, respectively. The extent of energy transfer is evident from the decrease in the donor intensity, and from the increase in acceptor intensity. There is considerable energy transfer in all the D-A pairs, ranging from ~75% for NU2D to 97% for TCD. In all cases the extent of energy transfer decreases as the length of the linker is increased.

Variation of the Förster Distance by Quenching. In order to obtain maximum resolution of the distance distribution, we use collisional quenching to decrease the quantum yield of the donors, which results in a decrease in the Förster distance and decreased energy transfer. This effect is illustrated in Figure 2C for NOA and NUD. The naphthalene emission was quenched using triethylamine (TEA). The peak intensities of the NOA emission, without TEA and with 0.6 and 1.5 M TEA, were normalized to the same peak intensity. The emission spectra of NUD are shown relative to the normalized intensities of NOA. As
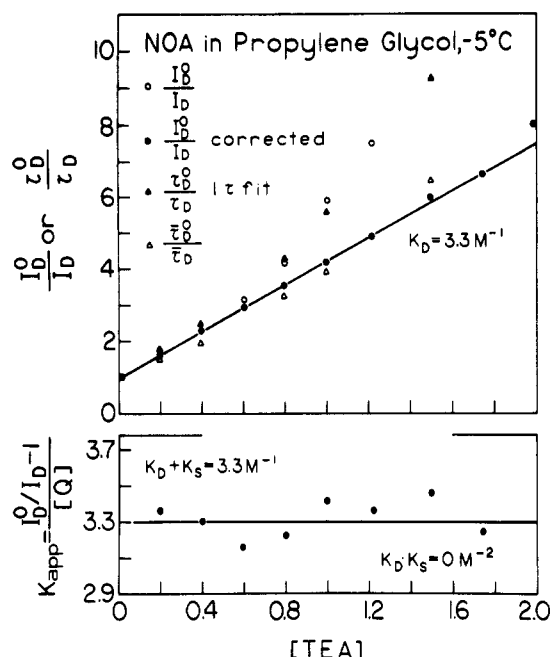
Figure 3. Quenching of NOA by TEA in propylene glycol at -5 °C. The uncorrected intensities (O) were corrected (●) for inner filter effects using $I_c = I_u 10^{OD/2}$, where I_u and I_c are the uncorrected and corrected values and OD is the optical density of the sample at the excitation wavelength. τ_D is the decay time from the best single-exponential fit and $\langle \tau_D \rangle = \Sigma_i f_i \tau_i$ from the best two- or three-exponential fits.

Table I
Dependence of the Förster Distance on Quencher Concentration

NOA Donor, -5 °C in Propylene Glycol

[TEA] (M)	$\phi_D{}^Q/\phi_D{}^\circ$	$\bar{\tau}_D{}^\circ/\bar{\tau}_D$	$R_o{}^Q$ (Å)
0	1.0	1.0[a]	23.45[b]
0.1			23.37
0.2	0.60	0.66	21.57
0.4	0.43	0.51	20.40
0.6	0.34	0.34	19.57
0.8	0.28	0.32	18.93
1.0	0.23	0.25	18.40
1.25	0.19	0.20	17.86
1.50	0.16	0.15	17.40
1.75	0.15		17.05

TMA Donor, 20 °C in Propylene Glycol

[acrylamide] (M)	$\phi_D{}^Q/\phi_D{}^\circ$	$\bar{\tau}_D{}^\circ/\bar{\tau}_D$	$R_o{}^Q$ (Å)
0	1.0	1.0	25.61
0.1	0.72	0.81	24.25
0.2	0.42	0.66	23.27
0.4	0.20	0.51	21.92
0.6	0.12	0.41	20.97
0.8	0.10	0.29	20.26
1.0	0.03	0.22	19.69
1.2	0.019		19.20

[a] The mean decay times $\bar{\tau}$ were calculated from the double-exponential fits (Tables II and III) using $\bar{\tau} = f_1\tau_1 + f_2\tau_2$. [b] The dynamic quenching constants were $K_D = 3.3$ M^{-1} for NOA and 3.85 M^{-1} for TMA. A static component was observed for TMA, $K_S = 0.95$ M^{-1}.

a result, the intensities at 340 nm for NUD represent the extent of energy transfer, independent of the extent of collisional quenching by TEA. The relative intensity of the donor increases in the presence of quencher, which indicates a decrease in the extent of energy transfer. A Stern–Volmer plot for the quenching of NOA by TEA is shown in Figure 3. The linearity of the plots of $I_D{}^\circ/I_D$ vs [Q] and the absence of a significant static component (lower panel) indicate that the quenching of NOA by TEA is primarily dynamic for our experimental conditions. We note that use of the best single-exponential fit decay times results in upward curvature of the Stern–Volmer plots, probably due to the short decay times induced by transient effects in quenching.[28–31] The Förster distance at each quencher concentration can be calculated from the dynamic component of the quenching (eqs 27–29). These values are summarized in Table I, as are the Förster distances for TMA quenched by acrylamide, calculated using eqs 27–29. In the case of TMA, there is a significant static component to the quenching, which must be separated using eq 28.

Frequency Response of the Donor Emission. In the absence of collisional quenching, the decays of the donors (TMA and NOA) are both close to a single exponential. This is seen by the overlap of the data with the calculated curves for the single-exponential model (leftmost curves in Figures 4 and 5) and the low values of $\chi_R{}^2$ for these fits (Tables II and III). However, the decays become more complex in the presence of quencher (rightmost curves), as can be seen from the failure of the single-exponential model (- - -) to fit the data and the elevated values of $\chi_R{}^2$. Examination of the single-exponential fits in Tables II and III reveals a progressive elevation of $\chi_R{}^2$ in the presence of increasing amounts of quencher. This increased heterogeneity in the donor decays is the result of transient effects in quenching, as has been observed previously in both the time[29] and the frequency domains.[30,31] Our distance distribution algorithm accounts for this increased heterogeneity by multiexponential parameterization in a
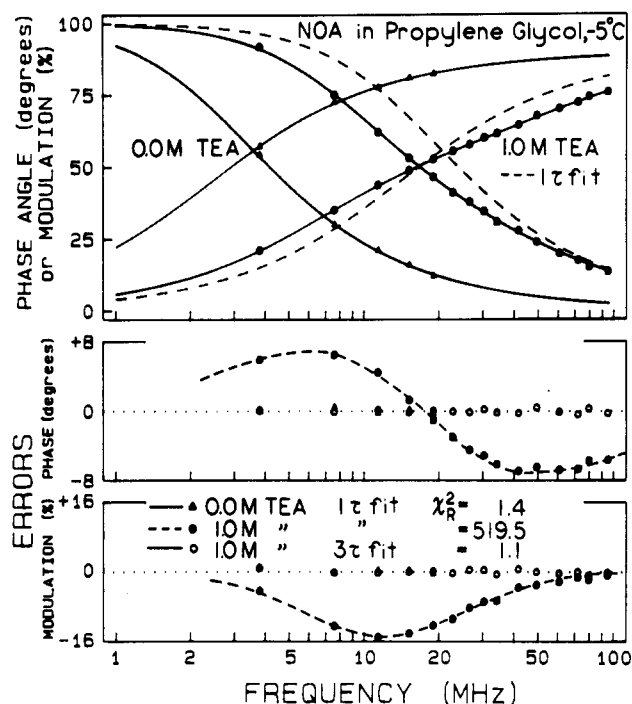

Figure 4. Frequency response of NOA without (▲) and with 1.0 M TEA (●). The dashed line (right) shows the best single-exponential fit to the emission of NOA in the presence of 1.0 M TEA. The solid line (left) is the best single-exponential fit to the NOA frequency response. The open circles (O) are the deviations from the three-exponential fit to the NOA decay with 1.0 M TEA.

manner which accurately reflects the frequency response. We found that the donor decay of quenched NOA required a triple exponential to obtain a good fit (Table II), whereas the decays of TMA were adequately described by a double exponential (Table III). It should be noted that the multiexponential analysis allows calculation of the mean decay time, which can be used to calculate the collisional component of the observed quenching. This can be seen in Figure 3 by the good agreement between the values of
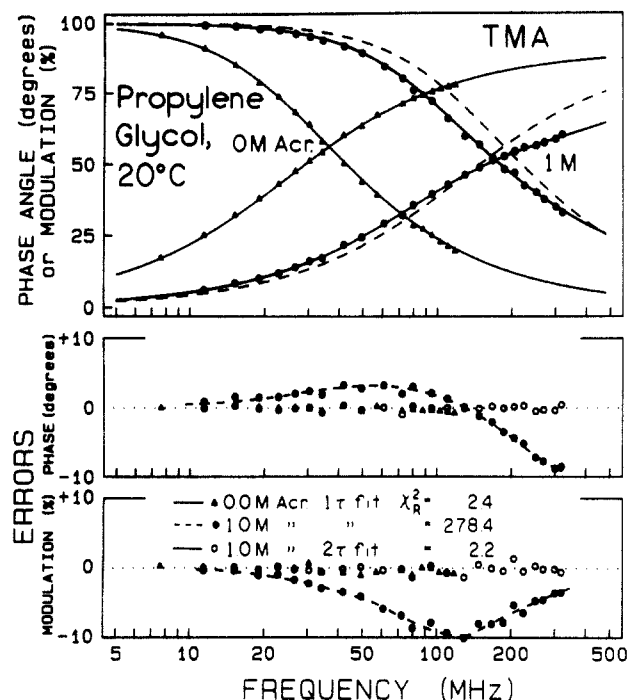
Figure 5. Frequency response of TMA without (▲) and with (●) 1.0 M acrylamide. The dashed line (right) shows the best single-exponential fit to the emission of TMA in the presence of 1.0 M acrylamide. The lower panels show the deviations from the one- and two-exponential models.

$\bar{\tau}_D{}^0/\bar{\tau}_D$ with the dynamic portion of the NOA quenching. In the case of acrylamide quenching of TMA, a static component is present, resulting in the relative quantum yields being smaller than the relative lifetimes (Table I). We previously demonstrated that the collisional contribution of the quenching yields the correct values of R_o.[9]

Frequency Response of D–A Pairs. The distribution of D–A distances for these flexible molecules is expected to result in increased heterogeneity in the frequency response of the donor emission. This effect is most easily seen in the donor decays of the D–A pairs when the donor decay is a single exponential, that is, in the absence of collisional quenching. One example is shown in Figure 6 for NOA and NUD. Addition of the dansyl acceptor results in a shift in the NOA donor frequency response to higher frequencies, which is due to the decrease in the donor decay time in the presence of a covalently linked acceptor. The donor decay of NUD is also seen to be extremely heterogeneous, as can be seen from our inability to fit the data to the single-exponential model (- - -) and the elevated value of minimized $\chi_R{}^2 = 1887$ for this model. Heterogeneous decays were also observed for the other D–A pairs, as shown in Figure 8 (Figure 7 for TCD and TU2D). The frequency response of the D–A pairs can be fit using the multiexponential model. These parameters are summarized in Tables IV and V for the naphthalene and tryptamine series, respectively. These data are provided to allow comparison of our results with future experiments or theoretical calculations. However, the multiexponential model does not reveal the parameters of interest, which are those describing the distribution of D-to-A distances.

Distance Distribution Analyses. We measured the frequency response of each donor or D–A pair at four to six quencher concentrations. The frequency responses of the D–A pairs were analyzed individually at each quencher concentration, and globally at all the quencher concentrations, to recover the distance distributions (values of $\bar{r}$ and half-width) which account for the data. In all cases the data could not be fit using a narrow distribution of

Table II
Multiexponential Analysis of the NOA Donor Decays with TEA Quenching, –5 °C in Propylene Glycol

[TEA] (M)	$\bar{\tau}$ (ns)[a]	τ_i (ns)	α_i	f_i	$\chi_R{}^2$
0.0	65.79	65.74	1.0	1.0	1.43
0.2		38.66	1.0	1.0	57.00
		10.12	0.166	0.043	
	43.55	45.05	0.834	0.957	1.99
0.4		26.43	1.0	1.0	293.75
		4.97	0.282	0.053	
		37.64	0.718	0.947	4.12
		2.99	0.160	0.018	
		9.74	0.182	0.068	
	33.76	36.16	0.658	0.914	2.74
0.8		14.92	1.0	1.0	428.35
		4.62	0.432	0.134	
		22.67	0.568	0.866	9.20
		2.09	0.198	0.089	
		8.94	0.402	0.248	
	21.70	26.28	0.400	0.734	2.33
1.0		11.49	1.0	1.0	519.5
		4.19	0.524	0.192	
		19.44	0.476	0.808	1.58
		2.13	0.111	0.021	
		5.05	0.497	0.199	
	16.70	20.07	0.442	0.780	1.08
1.2		7.67	1.0	1.0	660.7
		3.24	0.632	0.270	
		15.04	0.368	0.730	2.16
		1.88	0.182	0.046	
		4.08	0.490	0.266	
	12.05	15.78	0.328	0.689	1.42
1.5		6.68	1.0	1.0	547.8
		2.61	0.570	0.226	
		11.72	0.433	0.774	9.09
		0.99	0.206	0.032	
		4.19	0.496	0.328	
	10.11	13.61	0.297	0.640	2.28

[a] The mean decay time is calculated using $\bar{\tau} = \Sigma_i f_i \tau_i = \Sigma_i \alpha_i \tau_i{}^2$.

Table III
Multiexponential Analysis of the TMA Donor Decay with Acrylamide Quenching, 20 °C in Propylene Glycol

[AC] (M)	$\bar{\tau}$ (ns)[a]	τ_i (ns)	α_i	f_i	$\chi_R{}^2$
0		6.48	1.0	1.0	2.4
		0.38	0.048	0.003	
	6.53	6.54	0.952	0.997	1.2
0.2		4.03	1.0	1.0	53.5
		1.18	0.200	0.061	
	4.33	4.54	0.800	0.939	0.9
0.4		3.00	1.0	1.0	99.6
		0.79	0.265	0.075	
	3.32	3.52	0.735	0.925	1.0
0.6		2.24	1.0	1.0	143.1
		0.59	0.318	0.092	
	2.53	2.72	0.682	0.908	1.2
0.8		1.63	1.0	1.0	226.3
		0.39	0.436	0.125	
	1.91	2.13	0.564	0.875	1.7
1.0		1.27	1.0	1.0	278.4
		0.29	0.490	0.139	
	1.53	1.73	0.510	0.861	2.2

[a] The mean decay time is calculated using $\bar{\tau} = \Sigma_i f_i \tau_i = \Sigma_i \alpha_i \tau_i{}^2$.

distances. This is illustrated in Figure 7, where we attempted to fit the unquenched frequency response for NUD with a distance distribution in which half-width was held constant at 0.1 Å (- - -). However, the data could be fit if the half-width was allowed to vary (—). Similar results were observed for TCD and for TU2D (Figure 8), and once again the data could be fit to the Gaussian distribution model (—). The distance distribution parameters are summarized in Tables VI and VII, and the value of $\chi_R{}^2$ is nearly the same for the global fits as for the individual fits. Importantly, essentially the same parameters were recovered for each D–A pair at all concentrations of
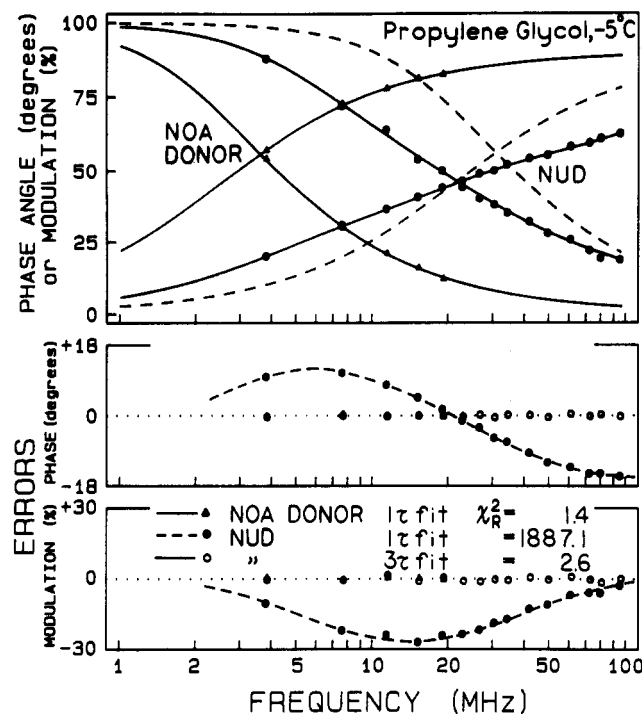
Figure 6. Frequency response of the donor emission from NOA and NUD. The dashed line (right) shows the best single-exponential fit to the donor emission of NUD.
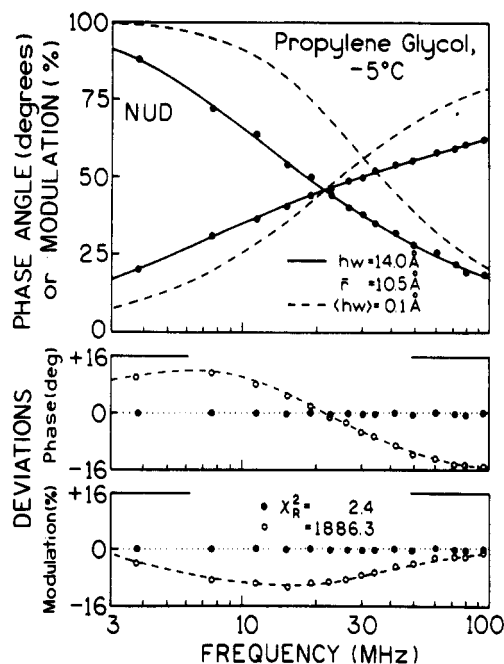

Figure 7. Distance distribution analysis of the donor emission of NUD. The solid line shows the best distance distribution fit, and the dashed line shows the distance distribution fit with the half-width held constant at 0.1 Å.

quencher (Tables VI and VII). Since the mean decay time is changed by quenching, these consistent parameters suggest that end-to-end diffusion does not have a significant effect on the donor decays.

The graphic results of the global analysis of progressively quenched D–A pairs are seen in Figure 9 for NUD (top) and for TU2D (bottom). The frequency response at all quencher concentrations is consistent with a single distance distribution, as is evident from the agreement between the calculated curves (—) and the data (●), and the acceptable values of χ_R^2 for the global analyses (Tables VI and VII). It is remarkable that the values of χ_R^2 from the global analysis are essentially the same as those from the
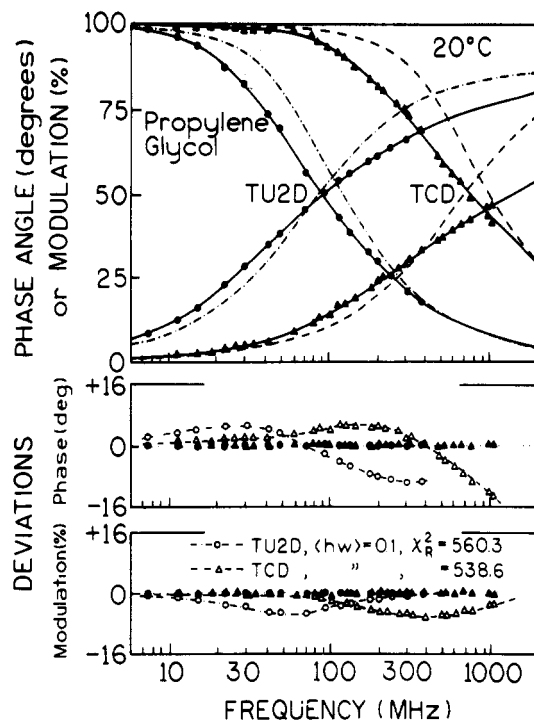

Figure 8. Distance distribution analyses for TCD and TU2D. The solid lines show the best distance distribution fit with $\bar{r}$ = 9.4 Å and a half-width (hw) of 11.1 Å for TCD and $\bar{r}$ = 19.5 Å and hw = 16.0 Å for TU2D. The dashed lines are the best fits with the half-width held constant at 0.1 Å.

Table IV
Multiexponential Analysis of the Donor Emission from NUD and NU2D, in the Absence of Quenching

D–A pair	$\bar{\tau}$ (ns)[a]	τ_i (ns)	α_i	f_i	χ_R^2
NUD		7.61	0.1	1.0	1887.1
		2.33	0.703	0.230	
		18.48	0.297	0.770	42.5
		1.43	0.550	0.116	
		7.62	0.327	0.367	
	17.6	28.47	0.123	0.516	2.61
NU2D		20.15	1.0	1.0	671.0
		6.55	0.500	0.161	
		34.16	0.500	0.839	7.09
		4.62	0.374	0.086	
		20.09	0.411	0.413	
	32.14	46.78	0.215	0.501	2.20

[a] The mean decay time is calculated using $\bar{\tau} = \Sigma_i f_i \tau_i = \Sigma_i \alpha_i \tau_i^2$.

individual analyses at each quencher concentration. Additionally, since the value of R_o is changed by quenching, the consistent distance distribution parameters suggest the recovered distribution is not sensitive to the precise range of the energy-transfer window. This should be regarded as strong evidence for the reliability of the recovered distributions.

The distance distributions recovered for all the D–A pairs are shown in Figure 10. As expected, the distributions are displaced to longer values of $\bar{r}$ as the length of the spacer is increased. Also, the distributions appear to become wider with increased length of the spacer. It is important to note that essentially the same values of $\bar{r}$ and half-width were obtained from the two series of D–A pairs for linkers of comparable length. This suggests that the distance distributions are characteristic of the flexible spacer and not the specific D–A pair used to measure the distribution. The slightly larger average distance for TUD (11.5 Å) vs NUD (10.7 Å) may be the result of the longer spacer for TUD (16 atoms) vs NUD (15 atoms). Although not shown, similar distributions were found for each D–A pair at various temperatures, usually lower temperatures

Table V
Multiexponential Analysis of the Donor Emission from TCD, TUD, and TU2D

D-A pair	$\bar{\tau}$ (ns)[a]	τ_i (ns)	α_i	f_i	χ_R^2
TCD		0.33	1.0	1.0	977.4
		0.15	0.857	0.456	
		1.07	0.143	0.544	16.2
		0.08	0.724	0.254	
		0.43	0.232	0.436	
	0.72	1.63	0.044	0.310	1.81
TUD		0.88	1.0	1.0	1494.4
		0.25	0.711	0.245	
		1.86	0.289	0.755	37.3
		0.20	0.641	0.179	
		1.32	0.332	0.621	
	1.92	5.29	0.027	0.200	1.1
TU2D		2.38	1.0	1.0	479.6
		0.67	0.480	0.150	
		3.50	0.520	0.850	7.2
		0.48	0.377	0.086	
		2.34	0.448	0.501	
	3.25	4.95	0.175	0.143	1.5

[a] The mean decay time is calculated using $\bar{\tau} = \Sigma_i f_i \tau_i = \Sigma_i \alpha_i \tau_i^2$.

Table VI
Distance Distribution Analysis of NUD and NU2D

D-A pair	[TEA] (M)	R_0^Q (Å)	E^Q SS	E^Q FD	$P(r)$ $\bar{r}$ (Å)	$P(r)$ hw (Å)	χ_R^2
NUD	0	23.45	0.92	0.92	10.5	14.0	2.4
	0.2	21.57	0.90	0.91	11.0	13.5	1.8
	0.4	20.46	0.88	0.89	10.8	13.6	1.2
	0.8	18.93	0.84	0.86	10.6	13.9	1.2
	1.0	18.40	0.83	0.85	10.8	13.6	1.2
NUD global	0-1.0				10.7	13.8	1.8
	0-1.0					⟨0.1⟩	1124.9
NU2D	0.0	23.45	0.75	0.74	18.1	14.3	1.8
	0.2	21.57	0.68	0.68	17.8	14.7	1.5
	0.4	20.40	0.64	0.64	17.8	14.3	1.2
	0.8	18.93	0.56	0.56	17.8	15.2	1.0
	1.0	18.40					
	1.2	17.86	0.52	0.50	18.0	14.8	1.9
NU2D global	0-1.2				17.9	14.5	2.2
						⟨0.1⟩	287.5

Table VII
Distance Distribution Analysis of TCD, TUD, and TU2D

D-A pair	[Ac] (M)	R_0^Q (Å)	E^Q SS	E^Q FD	$P(r)$ $\bar{r}$ (Å)	$P(r)$ hw (Å)	χ_R^2
TCD	0	25.61	0.97	0.98	9.4	11.1	2.5
	0.2	23.28	0.96	0.97	9.3	11.0	1.8
	0.4	21.92	0.95	0.97	8.1	12.1	2.2
	0.6	20.97	0.93	0.96	8.8	11.9	2.9
	0.8	20.26	0.92	0.95	8.0	12.2	2.3
TCD global	0.08				8.4	11.9	2.9
	0.08					⟨0.1⟩	597.9
TUD	0	25.61	0.93	0.94	11.7	14.6	1.3
	0.2	23.28	0.91	0.91	11.3	14.6	1.5
	0.4	21.92	0.88	0.89	11.7	14.3	1.1
	0.6	20.97	0.85	0.87	11.5	14.4	2.4
	0.8	20.26	0.84	0.85	11.9	14.1	2.1
	1.0	19.69	0.81	0.84	11.6	14.5	2.3
TUD global	0-1.0				11.5	14.6	2.4
	0-1.0		0.76	0.75		⟨0.1⟩	755.8
TU2D	0.0	25.61	0.76	0.75	19.5	16.0	1.9
	0.2	23.28	0.69	0.67	19.4	16.4	2.2
	0.4	21.92	0.66	0.62	19.6	15.2	1.6
	0.6	20.97	0.60	0.59	19.3	15.7	1.9
	0.8	20.26	0.56	0.56	19.0	16.5	2.7
	1.0	19.69	0.54	0.54	18.6	17.7	2.9
TU2D global	0-1.0		19.0		16.7		2.9
	0-1.0					⟨0.1⟩	915.9

to further minimize the effects of end-to-end diffusion.

We questioned the range of distance distributions that were consistent with the experimental data. More specifically, we examined the dependence of χ_R^2 on the values
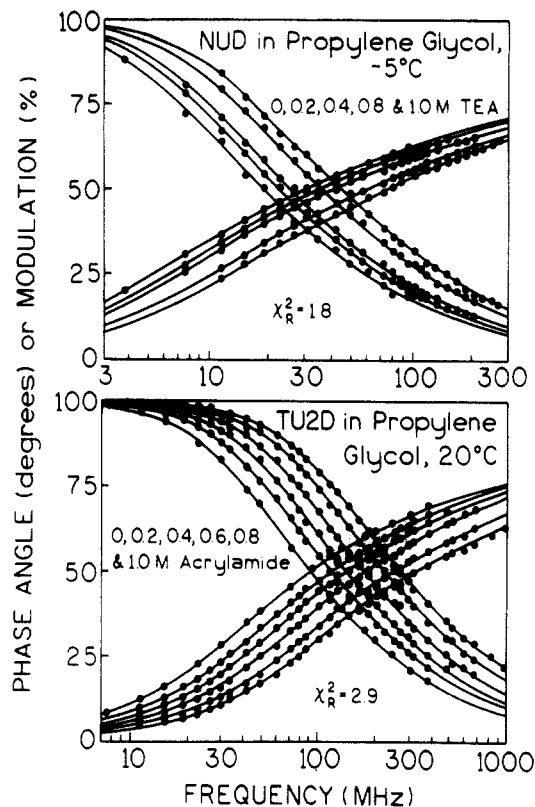
Figure 9. Top: Frequency response and global distance distribution analysis for NUD at five concentrations of TEA. The solid lines show the best global fit with $\bar{r}$ = 10.7 Å and hw = 13.5 Å. Bottom: Frequency response and global distance distribution analysis for TU2D at six acrylamide concentrations. The solid lines show the best global fit with $\bar{r}$ = 19.0 Å and hw = 16.7 Å, χ_R^2 = 2.7. The R_0^Q values are from Table I.
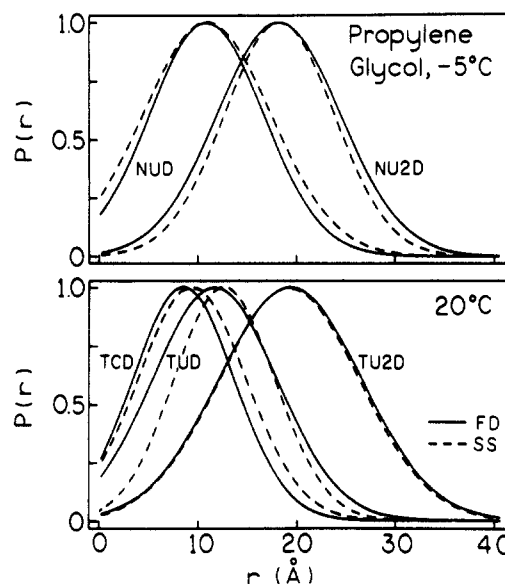
Figure 10. Distance distributions recovered from global analysis of the frequency-domain data (—) for the naphthalene (top) and the tryptamine series (bottom). Also shown (- - -) are the distance distributions recovered from the steady-state data.[8,9]

of $\bar{r}$ and half-width (hw). In these calculations of the χ_R^2 surfaces the other parameter (hw or $\bar{r}$) was allowed to vary as $\bar{r}$ or hw as held fixed at the values shown on the x-axis. In this way the χ_R^2 surfaces take into account the correlation between $\bar{r}$ and hw in determining the minimum values of χ_R^2. Remarkably, these χ_R^2 surfaces demonstrate that there is relatively little uncertainty in either $\bar{r}$ or hw for all the D-A pairs, with $\bar{r}$ being determined to within ~±0.3 and hw to within ±0.5. These estimates of the
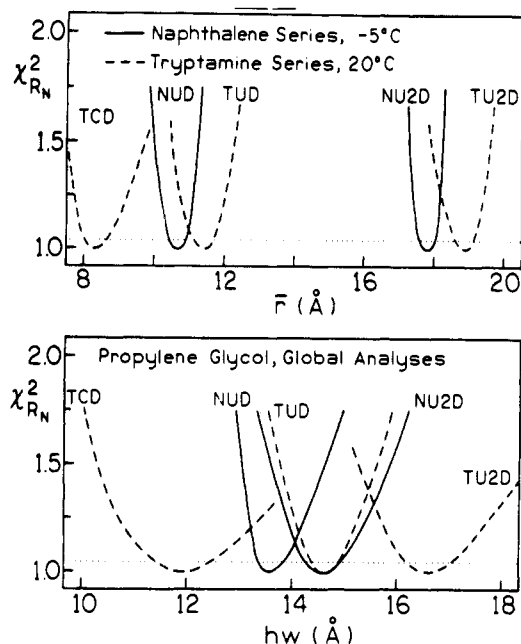
Figure 11. Distance distribution $\chi_R{}^2$ surfaces. All surfaces are calculated for the global fits, using the data available at all quencher concentrations. The intersection of these curves with the vertical dotted line represents the maximal range of $\bar{r}$ and hw values consistent with the FD data.
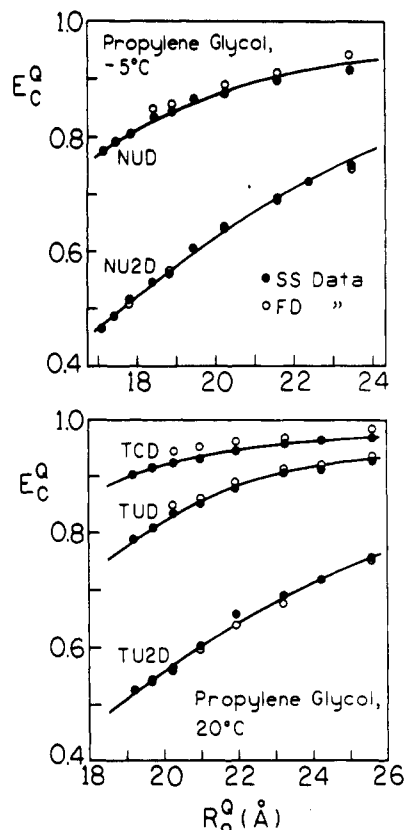

Figure 12. Energy-transfer efficiencies as observed from the steady-state emission (●) and as calculated from the FD distance distribution (O). Also shown are the best distance distribution fits to the steady-state data (—).

uncertainty are derived from the intersection of the $\chi_R{}^2$ surfaces with the maximum $\chi_R{}^2$ value consistent with random errors in 67% of repeated experiments. To the best of our knowledge, based on simulated data, this is an overestimate of the uncertainties.

Distance Distributions from Steady-State Transfer Efficiencies. The $\chi_R{}^2$ surface in Figure 11 indicate little uncertainty in the values of $\bar{r}$ and hw. However, we realized that the data did not define the shape or amplitude of the distributions at distances below ~ 10 Å. This lack of information for distances below 10 Å was revealed most clearly in attempts to fit the data to skewed Gaussian distributions, which allowed variable probabilities at short distances. This is an expected result because energy transfer is complete for the closely spaced D–A pairs, and these do not contribute to the measured frequency response. However, these closely spaced D–A pairs would be detected in the steady-state data, in that the emission from these molecules would be missing from the donor intensity values. Hence, we compared the measured steady-state transfer efficiencies (●) with those calculated from the distance distributions (O) obtained from the frequency-domain data (Figure 12). The range of R_o values was obtained by collisional quenching. If there were a significant population of closely spaced D–A pairs (dark complexes) then the steady-state transfer efficiencies would be higher than those calculated from the FD data. This was not observed (Figure 12), and the transfer efficiencies were in close agreement, suggesting the absence of D–A pairs spaced too close to be observed in the FD measurements.

Additionally, the steady-state transfer efficiencies for various values of R_o allow an independent determination of the distance distributions.[8,9] These distributions are shown in Figure 10 (- - -) and were found to be nearly identical with the distance distributions that were recovered from the FD data (—), again indicating the absence of a significant fraction of the D–A pairs so closely spaced as to be undetectable from the frequency-domain data.

Independent Prediction of $P(r)$. It is of interest to compare the experimentally recovered distance distribu-

tions with those predicted from conformational theories. To this end we implemented the rotational isomeric state model described by Flory[10] for the behavior of long, chainlike polymers. This theory allows prediction of the $P(r)$ distribution for these molecules based on the molecular parameters describing the flexibility behavior of the linker. We note that, depending upon one's confidence in the calculated or experimentally recovered distributions, the comparison can be used to refine the molecular parameters used to calculate the distribution or to refine the experimental methods.

In the RIS model the conformational space available to the molecule is simplified by fixing the bond lengths and angles at their equilibrium values and limiting the number of allowed rotational positions to low-energy minima. Three positions are allowed in the case of an alkyl chain, trans, gauche +, and gauche −; for an n-link chain this is a set of 3^{n-1} distinct conformations. In an equilibrium population of conformations, the probability of each isomer is related to that isomer's internal energy by the Boltzmann factor, $\exp(-E(c)/RT)$, where $E(c)$ is the estimated energy for that isomer, R is the universal gas constant, and T is the temperature in kelvin. In this model the total energy of the conformation is reckoned as the sum of contributions from each bond; further, these contributions depend only on the rotational position of that bond and the preceding one. The long-range interactions (such as the 1–4 hydrogen bonds in an α-helical section of a protein) are neglected. In the case of a typical alkyl chain, trans is 0 kcal/mol, gauche is ~ 0.5 kcal/mol, and gauche preceded by gauche of the opposite sign is penalized 2.0 kcal/mol.

Each rotational isomer is associated with a certain end-to-end distance (which is calculated directly) and an estimated conformational energy. The distance distribution function, $P(r)$, derived from this model is the

Table VIII
Parameters Used in Rotational Isomeric State Model[a]

bond number			bond geometry			bond energy	
TCD	TUD NUD	TU2D NU2D	length (Å)	angle (deg)	rot. angle	E_σ (P_σ)[b]	E_ω (P_ω)
1	1	1	1.85			0 (1.0)	0 (1.0)
2	2	2	1.82	120	2	0 (1.0)	0 (1.0)
3	3	3	1.62	109.5	3	0 (1.0)	0 (1.0)
4	4	4	1.46	109.5	3	0 (1.0)	0 (1.0)
5	5	5	1.53	112	3	0 (1.0)	1360 (0.10)
6	6	6	1.54	112	3	0 (1.0)	1360 (0.10)
	7–11	7–11, 18–22	1.54	112	3	498 (0.43)	1995 (0.035)
7	12	12, 23	1.54	112	3	498 (0.43)	556 (0.39)
8	13	13, 24	1.51	112	3	−200 (1.4)	∞ (0)
9	14	14, 25	2.38	142.6	3	397 (0.51)	0 (1.0)
10	15	15, 26	1.46	158.4	3	0 (1.0)	0 (1.0)
11	16^{TUD}	$16, 27^{TU2D}$	1.53	112	3	0 (1.0)	1360 (0.1)
	16^{NUD}	27^{NU2D}	1.53	112	3	0 (1.0)	0 (1.0)
12	17^{TUD}	$17, 28^{TU2D}$	1.54	112	3	0 (1.0)	1360 (0.1)
	17^{NUD}	28^{NU2D}	1.54	112	2	0 (1.0)	0 (1.0)
13	18^{TUD}	29^{TU2D}	1.56	152.6	3	0 (1.0)	0 (1.0)

[a] Bond 1 is the intra-dansyl bond. For sources see refs 35 and 36 and ref 10, pages 145–146. [b] The relative probabilities (P_σ and P_ω) are given by exp $(-E/RT)$ at 300 K.

Boltzmann-weighted histogram of the distance from this set of conformations. Consider the set of conformations, (c_j), and $E(c_j)$ as the estimated energy function and $d(c_j)$ as the end-to-end distance function evaluated at the jth conformation. Then the overall probability that r is in the ith distance interval from r_i to r_{i+1} is related to the sum of the probability terms, $\exp[-E(c_j)/RT]$, for each of the c_j which conform to the condition that the end-to-end distance is within that interval; this can be written mathematically as

$$P(r_i < r \leq r_{i+1}) = \frac{1}{Z} \sum_{c_j : r_i < d(c_j) \leq r_{i+1}} \exp[-E(c_j)/RT] \quad (33)$$

where the normalization factor Z is given by

$$Z = \sum_{\text{all } c_j} \exp[-E(c_j)/RT] \quad (34)$$

The number of possible conformations increases rapidly as the length of the alkyl linker is increased. Consequently, depending upon the size of the linker, it may be practical or practically impossible to calculate the energy of all possible conformations. For the shortest of the five molecules, TCD, a complete survey of all the rotational isomers is still practical. For the other molecules, the histogram was generated by picking a representative sample of conformations using a Monte Carlo selection, in which the probability of selection for a particular conformation is proportional to its energy weighing.[33,34] The sample size was sufficiently large so that it was apparent that the shape of the curve had converged to within a small tolerance. We also considered three simple conformational models. These were as follows: (1) the freely jointed (FJ) model, in which all restrictions on bond angles are removed; that is, all bond angles are equally likely; (2) the freely rotating (FR) model, in which the bond angles are fixed but all rotational positions are equally likely; and (3) the rotationally restricted (RR) but unweighted model, in which only three rotational positions are allowed but all are equally likely. This latter model corresponds to the high-temperature limit of the RIS model. In the RR and FR models, the bond angles are restricted to those used in the RIS model. The low-temperature limit of the RIS model is the global energy minimum "all trans" conformation. To generate the
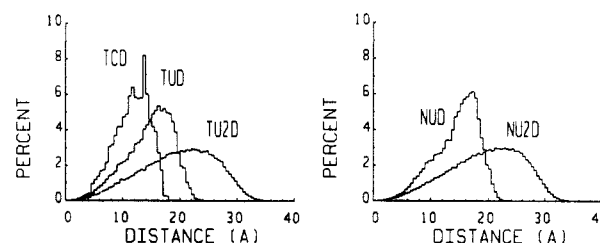

Figure 13. Distance distribution histograms obtained using the RIS model and the parameters in Table VIII.
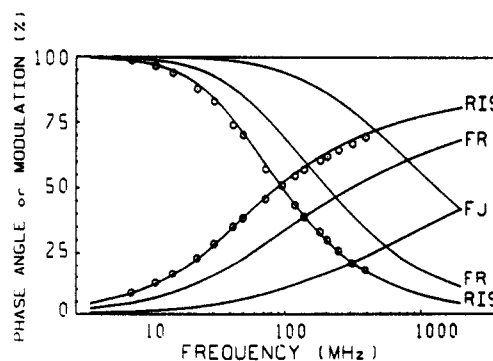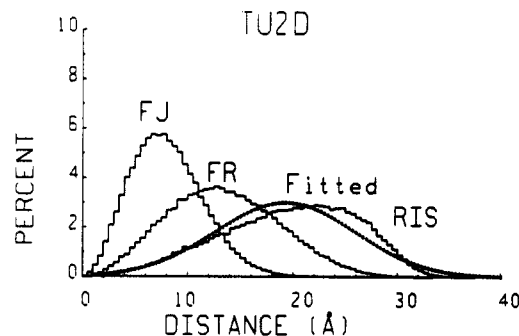

Figure 14. Comparison of the RIS, FR, and FJ histograms for TU2D, and the experimental distribution (···). The lower panel shows the experimental frequency response (O), and that predicted from the RIS, FR, and FJ histograms.

histograms corresponding to these simpler models, an ordinary random sampling procedure was used. It was found that the RR and FR models produce essentially indistinguishable distance distribution functions (not shown), so only the RIS, FR, and FJ results will be discussed.
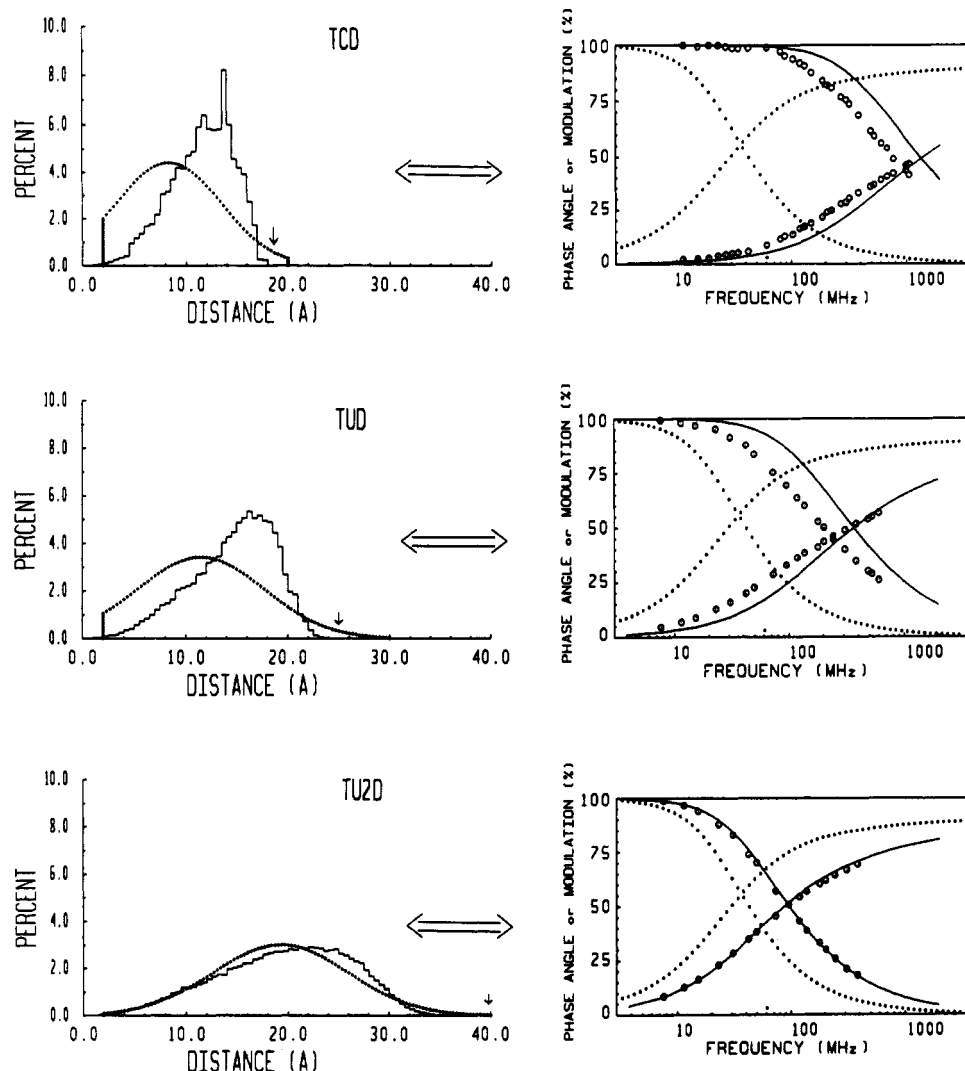
Figure 15. Left: Comparison of the RIS-derived distance histograms (—) with the experimental distance distributions (⋯) for the tryptamine series of D–A pairs. Right: Frequency responses for the donor alone (⋯) and for the D–A pairs (O) and that predicted from the RIS histogram (—). The arrows indicate the maximum D-to-A distance consistent with the structural parameters (Table VIII). The Gaussians are truncated beyond the distance used in fitting the data.

The input parameters which are used in the simulation are themselves somewhat uncertain (see Table VIII and references therein). The particular values which were used are given in Table VIII as well as the relative Boltzmann factors 300 K. A small effect of temperature could be seen in the simulations at 300 K as compared to the experimental temperatures of 268 (–5 °C and 293 K (20 °C). However, these effects were minimal (not shown).

Simulation Results. Conformational analysis for the five molecules using the RIS model yields the $P(r)$ histograms shown in Figure 13. These calculated distance distributions are unimodal, with increasing values for the peak position and half-width as the chain increases in length. In this respect, the results of the simulation are in agreement with the experimentally recovered distributions shown in Figure 10. We questioned whether the simpler models (freely jointed and freely rotating) provide reasonable predictions of the end-to-end distribution. This comparison is shown in Figure 14 for TU2D, along with the experimental distributions. Evidently, these simpler models do not provide useful estimates of the end-to-end distributions. In particular, removal of the restriction on bond angles (freely jointed model) results in a much shorter distribution. Restriction of the bond angles in the freely rotating model results in improved agreement with experiment. However, the best match between theoretical and experimental distributions was obtained using the

RIS model (Figure 14). Further experimentation and analysis is needed to see if the RIS and experimental distributions can be improved by variation of the energetics of the various conformational states.

It is of interest to compare the actual experimental data with that predicted from the calculated distributions. This was accomplished by using the $P(r)$ obtained by eq 33 in eqs 25 and 26. This comparison is shown in Figure 14 for TU2D. It is clear that the freely jointed and freely rotating models predict too much energy transfer, as is seen from the calculated frequency responses being displaced toward higher frequencies relative to the experimental results. In contrast, the frequency response predicted from the RIS is in good agreement with the experimental response. Hence, in the case of a moderately long linker, the predictions of the RIS model appear to be in excellent agreement with our experimental results.

Since the RIS model appeared to successfully predict the end-to-end distribution of TU2D, we questioned whether this model would be equally successful for the shorter D–A pairs. This comparison is shown in Figure 15 for the tryptamine series, and in Figure 16 for the naphthalene series. One notices that the RIS model and experiment are in reasonable agreement for the longest D–A pairs (TU2D and NU2D), but that the agreement is progressively worse for the middle (TUD and NUD) and shortest (TCD) D–A pairs. In all cases, and especially for
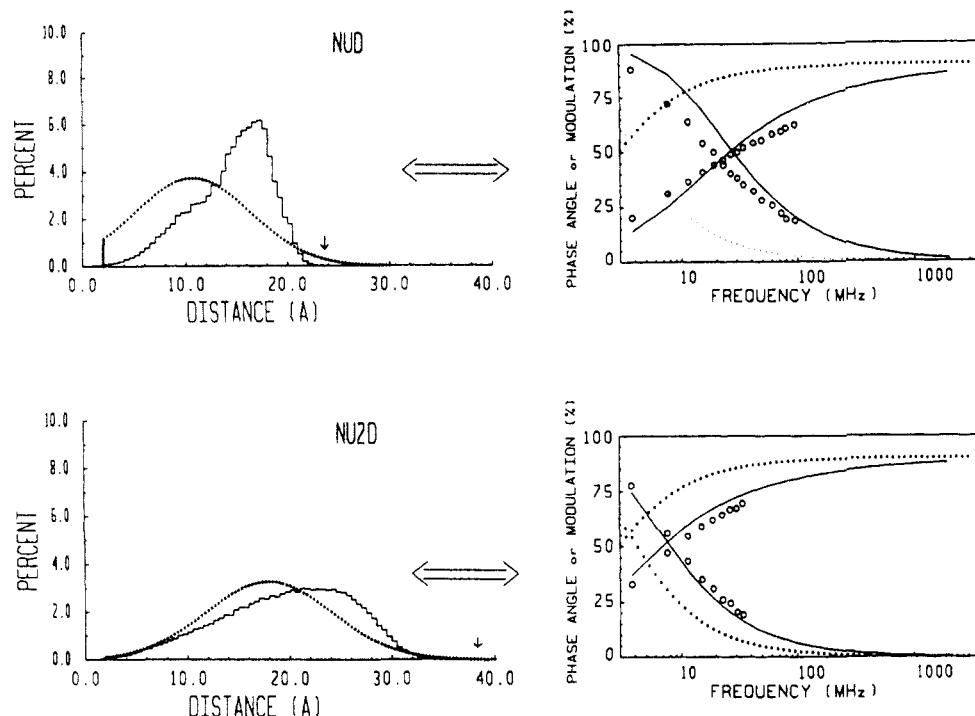
Figure 16. Left: Comparison of the RIS-derived distance histograms (—) and the experimental distance distributions (···) for the naphthalene series of D-A pairs. Right: Frequency responses for the donor alone (···) and for the D-A pairs (O) and that predicted from the RIS histogram (—). The arrows indicate the maximum D-to-A distance consistent with the structural parameters (Table VIII). The Gaussians are truncated beyond the distance used in fitting the data.

the shortest D-A pair, the calculated histograms appear to be skewed Gaussians, whereas a symmetrical Gaussian was adequate to account for the experimental data.

This pattern of disagreement is also seen when the measured and predicted frequency responses are compared (Figures 15 and 16, right). In this comparison one accounts for the differential sensitivity of the energy-transfer measurements along the distance axes, and how these populations contribute to the frequency response. The same pattern of agreement or disagreement was found, with the calculated frequency responses diverging from the experimental data as the linker became shorter. This suggests that the experimental data for the shorter D-A pairs are in fact not consistent with the predictions of the RIS model and thus suggests the inadequacy of this model for short alkyl chains. The pattern of agreement or disagreement, that is, the relative curve shapes, persists at all quencher concentrations (not shown). Additionally, we note that we were not able to improve the fit to the data using a skewed Gaussian;[23] that is, the goodness of fit was not improved by inclusion of the additional skewness parameter. This suggests that we have obtained an adequate description of the actual distance distribution and suggests an inadequacy of the RIS model for predicting the distance distributions of short alkyl chains.

Discussion

Time-resolved measurements of energy transfer, as measured in either the time or frequency domain, provide unique information on the conformational distribution of flexible molecules. Importantly, the data contain information on the distribution of donor-to-acceptor distances, which in turn allows direct comparison with theories for the statistical mechanics of chain molecules.[10] We note that our frequency-domain measurements allow resolution of the actual distance distribution and comparison with predicted distributions. In contrast, steady-state data only allow comparison of average extent of energy transfer.[37] In the present paper we increased the resolution of the

experiments by using collisional quenching to obtain a range of Förster distances. Additionally, we further constrained the recovered distance distributions using the steady-state transfer efficiencies, which are sensitive to closely spaced D-A pairs that would not be observed in the time-resolved measurements.

Comparison of the experimentally determined distance distributions revealed surprisingly good agreement with that calculated from the RIS model[10] for the longest linkers (~28 atoms). However, the measured and calculated (RIS) distributions were in poor agreement for the short linker (11 atoms). One should consider the variety of factors related to the assumptions of the model that may interfere with a direct comparison of theory and measurement. We note that the RIS model ignores long-range interactions and assumes that the molecules are in a good solvent. Also, there is no consideration of possible stacking interactions between the chromophores, although this is unlikely based on the steady-state data. The energy level, distance, and end-point position parameters that were used within the chromophores may be inaccurate descriptions of the end-group behavior. Consideration of such factors may allow refinement of the theory for conformational analysis, or refinement of the energy parameters, and thereby improve the conformational calculations for these and other polymers or biopolymers.

Appendix

Selection of the Gaussian Distance Distribution $P(r)$. In his classic work Flory[10] discussed the vector distance distribution function $W(r)$ for infinite chains with various conformational constraints. However, to the best of our knowledge, expressions do not exist to describe the end-to-end distributions of the finite-length molecules described in the report. Hence, we chose the one-dimensional Gaussian distribution (eq 9). To avoid confusion, it seems appropriate to describe the relationship between our empirical model and Flory's model.

For a long freely jointed polymeric chain, the end-to-end distribution of distances is equivalent to that obtained from a random walk in space. If one puts the first end at the origin and considers the end-to-end vector, **r**, then for large values of n the probability density function describing the probability of finding the other end within volume element dv at position r is given by

$$W(r) \, dv = A \exp\left(\frac{-|\mathbf{r}|^2}{B}\right) = A \exp\left(\frac{-r^2}{B}\right) \quad (A1)$$

where A and B are constants. Since for large n the probability density is spherically symmetric, the probability of finding the other end within a volume element may be determined by integrating over the spherical shell defined by $r \leq |\mathbf{r}| \leq r + dr$. Hence, our $P(r)$ is related to Flory's $W(r)$ by

$$P(r) \, dr = \int_{r \leq |\mathbf{r}| \leq r+dr} W(r) \, dv = 4\pi r^2 A \exp\left(\frac{-r^2}{B}\right) dr \quad (A2)$$

The new constant terms can be absorbed into the preexponential factor to emphasize that the net change is the addition of the r^2 factor

$$P(r) \, dr = A' r^2 \exp\left(\frac{-r^2}{B}\right) dr \quad (A3)$$

In a previous report,[38] we demonstrated that the shape of the end-to-end distribution was not affected by the use of r^2 in the distribution functions. Of course, the parameters describing the distribution functions were different, but the overall shape was unchanged.

In the present report we are dealing with donors and acceptors linked by finite length spacers. This results in at least two difficulties in selecting the distribution function. First, the mean D–A distance will be nonzero because of the finite size of the donor and acceptor and because of steric constraints imposed by the finite length linker. Second, not all of the three-dimensional space is available to the acceptor. This later point is clarified by recalling the linker is initially directed away from the donor in a single direction. There exists the probability that the spatial distribution is not radially symmetric about the origin, particularly for the shorter chains like the linker in TCD. On the basis of these considerations, we are required to allow for a nonzero mean, and the choice of a volume element $(4\pi r^2 \, dr)$ in eq A2) is not clear.

Conceding that these alterations (probability density function is not centered at the origin and is not radially symmetric) are superimposed on the Gaussian density function describing the limit (as n approaches infinity) of the end-to-end distribution function for a freely jointed chain, we arrived at the two-parameter probability distribution fitting function described in the paper ($B = 2\sigma^2$; Z_{Gau} is the normalization constant)

$$P(r) = \frac{1}{Z_{\text{Gau}}} \exp\left[-\frac{1}{2}\left(\frac{r - \bar{r}}{\sigma}\right)^2\right] \quad (A4)$$

References and Notes

(1) Stryer, L. *Annu. Rev. Biochem.* **1978**, *47*, 819–846.
(2) Steinberg, I. Z. *Annu. Rev. Biochem.* **1971**, *40*, 83–114.
(3) Lakowicz, J. R. *Principles of Fluorescence Spectroscopy*; Plenum Press: New York, 1983; Chapter 10, pp 303–339.
(4) Förster, Th. *Ann. Phys. (Leipzig)* **1948**, *2*, 55–75 (Translated by R. S. Knox, University of Rochester).
(5) Gratton, E.; Limkeman, M. *Biophys. J.* **1983**, *44*, 315–324.
(6) Lakowicz, J. R.; Maliwal, B. P. *Biophys. Chem.* **1985**, *21*, 61–78.
(7) Lakowicz, J. R.; Laczko, G.; Gryczynski, I. *Rev. Sci. Instrum.* **1986**, *57*, 2499–2506.
(8) Gryczynski, I.; Wiczk, W.; Johnson, M. L.; Lakowicz, J. R. *Chem. Phys. Lett.* **1988**, *145*, 439–446.
(9) Gryczynski, I.; Wiczk, W.; Johnson, M. L.; Cheung, H. C.; Wang, C. K.; Lakowicz, J. R. *Biophys. J.* **1988**, *54*, 577–586.
(10) Flory, P. *Statistical Mechanics of Chain Molecules*; John Wiley and Sons: New York, 1969.
(11) Lakowicz, J. R.; Kusba, J.; Wiczk, W.; Gryczynski, I.; Szmacinski, H.; Johnson, M. L. *Biophys. Chem.* **1991**, *39*, 79–84.
(12) Lakowicz, J. R.; Kusba, J.; Wiczk, W.; Gryczynski, I.; Johnson, M. L. *Chem. Phys. Lett.* **1990**, *173*, 319–326.
(13) Haas, E.; Wilchek, H.; Katchalski-Katzir, E.; Steinberg, I. Z. *Proc. Natl. Acad. Sci. U.S.A.* **1975**, *72*, 1807–1811.
(14) Amir, D.; Haas, E. *Biopolymers* **1986**, *25*, 235–240.
(15) Haas, E.; Katchalski-Katzir, E.; Steinberg, I. Z. *Biopolymers* **1978**, *17*, 11–31.
(16) Katchalski-Katzir, E.; Steinberg, I. Z. *Ann. N.Y. Acad. Sci.* **1981**, *366*, 41–61.
(17) Reference deleted in proof.
(18) Dale, R. E.; Eisinger, J.; Blumberg, W. E. *Biophys. J.* **1979**, *26*, 161–193.
(19) Haas, E.; Katchalski-Katzir, E.; Steinberg, I. Z. *Biochemistry* **1978**, *17*, 5064–5070.
(20) Lakowicz, J. R.; Johnson, M. L.; Wiczk, W.; Bhat, A.; Steiner, R. F. *Chem. Phys. Lett.* **1987**, *138*, 587–593.
(21) Lakowicz, J. R.; Gryczynski, I.; Cheung, H. C.; Wang, G.; Johnson, M. L. *Biopolymers* **1988**, *27*, 821–830.
(22) Bevington, P. R. *Data Reduction and Error Analysis for the Physical Sciences*; McGraw Hill Inc.: New York, 1969; p 336.
(23) Wiczk, W.; Eis, P. S.; Fishman, M. N.; Johnson, M. L.; Lakowicz, J. R. *J. Fluoresc.* **1991**, *1*, 273–286.
(24) Lakowicz, J. R.; Gratton, E.; Laczko, G.; Cherek, H.; Limkeman, M. *Biophys. J.* **1984**, *46*, 463–477.
(25) Gratton, E.; Lakowicz, J. R.; Maliwal, B.; Cherek, H.; Laczko, G.; Limkeman, M. *Biophys. J.* **1984**, *46*, 479–486.
(26) Johnson, M. L. *Biophys. J.* **1983**, *44*, 101–106.
(27) Johnson, M. L.; Frasier, S. G. *Methods Enzymol.* **1985**, *117*, 301–342.
(28) Keizer, J. *J. Am. Chem. Soc.* **1983**, *105*, 1494–1498.
(29) Nemzek, T. L.; Ware, W. R. *J. Chem. Phys.* **1975**, *62*, 447–489.
(30) Joshi, N.; Johnson, M. L.; Gryczynski, I.; Lakowicz, J. R. *Chem. Phys. Lett.* **1987**, *135*, 200–207.
(31) Lakowicz, J. R.; Johnson, M. L.; Gryczynski, I.; Joshi, N.; Laczko, G. *J. Phys. Chem.* **1987**, *91*, 3277–3285.
(32) Chen, R. F. *Anal. Biochem.* **1967**, *1*, 35–42.
(33) Metropolis, N. A.; Rosenbluth, A. W.; Rosenbluth, M. N.; Teller, A. H.; Teller, E. *J. Chem. Phys.* **1953**, *21*, 1087–1092.
(34) Premilat, S.; Hermans, J., Jr. *J. Chem. Phys.* **1973**, *599*, 2602–2612.
(35) *Handbook of Chemistry and Physics*, 66th ed.; CRC Press, Inc.: Boca Raton, FL, 1985; pp F-165–F166.
(36) Wyckoff, R. W. G. *Crystal Structures*; John Wiley & Sons: New York, 1966; pp 53, 288, 682.
(37) Valeur, B.; Mugnier, J.; Pouget, J.; Bourson, J.; Santi, F. *J. Phys. Chem.* **1989**, *93*, 6073.
(38) Lakowicz, J. R.; Johnson, M. L.; Wiczk, W.; Bhat, A.; Steiner, R. F. *Chem. Phys. Lett.* **1987**, *138*(6), 587–593.
(39) Zimmt, M. B.; Peterson, K. A.; Fayer, M. D. *Macromolecules* **1988**, *21*, 1145–1154.